

Analysis of Peculiarities of the Stellar Velocity Field in the Solar Neighborhood

V.V. Bobylev¹, A.T. Bajkova¹, and A. A. Mylläri²

¹*Pulkovo Astronomical Observatory, Russian Academy of Sciences, St-Petersburg*

²*Turku University, Turku, Finland*

Abstract—Based on a new version of the Hipparcos catalogue and an updated Geneva-Copenhagen survey of F and G dwarfs, we analyze the space velocity field of ≈ 17000 single stars in the solar neighborhood. The main known clumps, streams, and branches (Pleiades, Hyades, Sirius, Coma Berenices, Hercules, Wolf 630- α Ceti, and Arcturus) have been identified using various approaches. The evolution of the space velocity field for F and G dwarfs has been traced as a function of the stellar age. We have managed to confirm the existence of the recently discovered KFR08 stream. We have found 19 Hipparcos stars, candidates for membership in the KFR08 stream, and obtained an isochrone age estimate for the stream, 13 Gyr. The mean stellar ages of the Wolf 630- α Ceti and Hercules streams are shown to be comparable, 4–6 Gyr. No significant differences in the metallicities of stars belonging to these streams have been found. This is an argument for the hypothesis that these streams owe their origin to a common mechanism.

DOI: 10.1134/S1063773710010044

INTRODUCTION

Studying the stellar velocity field in the solar neighborhood is of great importance in understanding the kinematics and evolution of various structural components in the Galaxy. At present, it is well known that the stellar space velocity distribution has a complex small-scale structure. This may be attributable to various dynamical factors (the influence of a spiral density wave, the Galactic bar, etc.).

The stellar velocity field in the solar neighborhood was analyzed by Chereul et al. (1998), Dehnen (1998), Asiain et al. (1999), Skuljan et al. (1999), and Torra et al. (2000) using Hipparcos (ESA 1997) data. The space velocities of K and M giants were studied by Famaey et al. (2005) using data from the Hipparcos and Tycho-2 (Hog et al., 2000) catalogues in combination with the radial velocities measured by the CORAVEL spectrovelocimeter. Based on data from the first version of the Geneva-Copenhagen survey (Nordström et al., 2004), Bobylev and Bajkova (2007a) analyzed the space velocities of F and G dwarfs as a function of the stellar age. Antoja et al. (2008) studied an extensive sample of stars of various spectral types, from O to M, using the stellar ages and space velocities.

The theory of stellar streams has long been used to explain the nature of the observed inhomogeneity of the stellar velocity field. Therefore, the names to the peaks were given by association with open star clusters (OSCs), such as the Pleiades (with an age of 70–125

Myr; Soderblom et al. 1993), the Sirius-Ursa Majoris cluster (500 Myr; King et al. 2003), or the Hyades (650 Myr; Castellani et al. 2001).

The theory of stellar streams suggests a common origin of the stars in a specific stream (Eggen 1996). The clumpy structure of the observed velocity field in the solar neighborhood is explained by a superposition of stars belonging to different streams.

As numerical simulations of the dynamical evolution of such OSCs as the Hyades, the Pleiades, and Coma Berenices show (Chumak et al. 2005; Chumak and Rastorguev 2006a, 2006b), stellar tails elongated along the Galactic orbit of the cluster appear during their evolution. However, in a time ≈ 2 Gyr, the OSC remnants existing in the form of tails must completely disperse and mix with the stellar background (Küpper et al. 2008).

The theory of stellar streams runs into great difficulties in explaining the existence of peaks or clumps in velocity space containing old (older than 2–4 Gyr) stars. Analysis of the stellar metallicities performed by Taylor (2000) for nine old streams (Hercules, Wolf 630, 61 Cyg, Arcturus, HR 1614, and others) composed according to Eggen's lists showed such a large spread in metallicity that a common origin of the stars in each of the streams is out of the question. With regard to HR 1614, there is still the opinion based on the chemical homogeneity of the stars that this is an OSC remnant with an age of about 2 Gyr (De Silva et al. 2007).

In recent years, nonaxisymmetric models of the Galaxy (a spiral structure, a bar, a triaxial halo) have been invoked to account for peculiarities in the distribution of stellar velocities in the solar neighborhood. For example, the Galactic spiral structure gives rise to clumpiness in the observed velocity field (De Simone et al. 2004; Quillen and Minchev 2005). The bar at the Galactic center (Dehnen 1999, 2000; Fux 2001; Chakrabarty 2007) leads to a bimodal distribution of the observed UV velocities.

At present, clumps of a completely different nature to which the Sirius, Hercules, and Arcturus streams belong are distinguished.

In the opinion of Klement et al. (2008), the Sirius stream contains not only stars formed simultaneously and evolving as an OSC but also a sizeable fraction of field stars that fell into this region through the impact of a spiral density wave.

Numerical simulations have shown that the existence of the Hercules stream ($V \approx -50$ km s⁻¹) can be explained by the fact that its stars have resonant orbits induced by the Galactic bar (Dehnen 1999, 2000; Fux 2001). In this case, the Sun must be located near the outer Lindblad resonance. A detailed analysis performed by Bensby et al. (2007) using high-resolution spectra of nearby F and G dwarfs showed this stream to contain stars of various ages, metallicities, and elemental abundances. Bensby et al. (2007) concluded that the influence of a bar-type dynamical factor is the most acceptable explanation for the existence of the Hercules stream.

Several authors (Navarro et al. 2004; Helmi et al. 2006; Arifyanto and Fuchs 2006) concluded that the Arcturus stream ($V \approx -100$ km s⁻¹) is the old (≈ 15 Gyr) debris of a dwarf galaxy captured by the Galaxy and disrupted by its tidal effect. Data on the kinematics and metallicities of the stars being analyzed served as arguments for this conclusion.

Analysis of the RAVE DR1 experimental data (Steinmetz et al. 2006) revealed a hitherto unknown stream (Klement et al. 2008) with an age of ≈ 13 Gyr in the region of “rapidly flying” stars ($V \approx -160$ km s⁻¹) whose origin has not yet been established.

The goal of this paper is to analyze peculiarities of the stellar velocity field in the solar neighborhood based on a new version of the Hipparcos catalogue, the OSACA and PCRV catalogs of radial velocities, and an updated Geneva-Copenhagen survey of F and G dwarfs,

which provide the currently most accurate data on the individual distances, space velocities, and ages of stars.

THE COORDINATE SYSTEM

In this paper, we use a rectangular Galactic coordinate system with the axes directed away from the observer toward the Galactic center ($l = 0^\circ$, $b = 0^\circ$, the X axis), along the Galactic rotation ($l = 90^\circ$, $b = 0^\circ$, the Y axis), and toward the North Galactic Pole ($b = 90^\circ$, the Z axis). The corresponding space velocity components of the object U , V , and W are also directed along the X , Y , and Z axes.

THE DATA

We use stars from the Hipparcos catalog (ESA 1997). We took the proper-motion components and parallaxes from an updated version of the Hipparcos catalog (van Leeuwen 2007), the stellar radial velocities from the OSACA compilation catalog of radial velocities (Bobylev et al. 2006) and the Pulkovo Compilation of Radial Velocities (Gontcharov 2006); improved age estimates and metallicity indices $[\text{Fe}/\text{H}]$ for F and G dwarfs were taken from an updated Geneva-Copenhagen survey (Holmberg et al. 2007, 2008).

As a result, we have data of various quality on 34359 stars of various spectral types. Among them, 16737 stars are single ones with the most reliable distance estimates, i.e., $e_\pi/\pi < 0.1$ for them. We chose the constraint on the parallax errors from the considerations of selecting a sufficiently large number of stars at the minimal effect of Lutz and Kelker (1973). These stars constitute our main working sample that we designate as “all” (Figs. 1, 2, 4, 5). The stellar UV-velocity distribution for this sample is presented in Fig. 1a.

For the selected stars, we, nevertheless, made a statistical estimate of the U and V velocity biases caused by the measurement errors of the stellar parallaxes. For this purpose, we used the method of Monte Carlo simulations. We generated 1000 random realizations of parallax errors for each star that satisfied a normal law. Figures 1b and 1c present the derived histograms separately for the U and V velocities, respectively. The number of stars whose velocity bias lies in a certain bin along the horizontal axis is indicated along the vertical axis. As we see from the histograms, the statistical U and V velocity biases caused by the parallax errors are generally insignificant; for 70% of the stars, they lie in the interval $[-0.05, 0.05]$ km s^{-1} . The maximum bias (given the asymmetry of the derived distributions) does not exceed 0.5 km s^{-1} . This value is approximately a factor of 2–3 lower than the statistical uncertainty caused by the measurement errors of the proper motions and radial velocities (Skuljan et al. 1999).

The stellar velocities were corrected for the differential rotation of the Galaxy. The Galactic differential rotation effect is known to manifest itself in its influence on the U velocity via the gradient $dU/dY = -\Omega_0$, then $\Delta U = (dU/dY)Y = -\Omega_0 Y$, where $\Omega_0 = B - A \approx -30 \text{ km s}^{-1} \text{ kpc}^{-1}$. This means that for a typical error in the stellar space velocities of $\varepsilon = 1 \text{ km s}^{-1}$, this effect may be disregarded only for the stars within $d < \varepsilon/\Omega_0 = 33 \text{ pc}$. Since the stars used also have greater distances, the differential rotation of the Galaxy should be taken into account.

The Galactic rotation parameters (the Oort constants A and B) have been repeatedly determined by various authors (Zabolotskikh et al. 2002; Olling and Dehnen 2003; Bobylev

2004); they are known with an error $\sigma \approx 1 \text{ km s}^{-1} \text{ kpc}^{-1}$. This means that for a typical error in the stellar space velocities of $\varepsilon = 1 \text{ km s}^{-1}$, the influence of an uncertainty in determining Ω_0 is significant for the stars located at distances $d > \varepsilon/3\sigma = 333 \text{ pc}$. Fortunately, the number of such distant stars in our “all” sample is small (only two or three dozen OB stars), and their influence may be neglected. In this paper, we use the Oort constants $A = 13.7 \pm 0.6 \text{ km s}^{-1} \text{ kpc}^{-1}$ and $B = -12.9 \pm 0.4 \text{ km s}^{-1} \text{ kpc}^{-1}$ that were determined by Bobylev (2004) from an analysis of the independent estimates obtained by various authors.

THE METHODS

The Adaptive Kernel Method

We use an adaptive kernel method to obtain an estimate of the velocity distribution $f(U, V)$ similar to that of the probability density distribution from the initial velocity distribution presented in Fig. 1. In contrast to the approach of Skuljan et al. (1999), we use a two-dimensional, radially symmetric Gaussian kernel function expressed as

$$K(r, \sigma) = \frac{1}{2\pi\sigma^2} \exp\left(-\frac{r^2}{2\sigma^2}\right), \quad (1)$$

where $r^2 = x^2 + y^2$ and σ is a positive bandwidth parameter; in this case, the relation $\int K(r)dr = 1$ needed to estimate the probability density holds. Obviously, the larger the parameter σ , the larger the bandwidth and the lower the amplitude.

The basic idea of the adaptive kernel method is that at each point of the map, the operation of convolution with a band of the width specified by the parameter σ that varies in accordance with the data density near this point is performed. Thus, in zones with an enhanced density, the smoothing is done by a comparatively narrow band; the bandwidth increases with decreasing data density.

We will use the following definition of the adaptive kernel estimator at an arbitrary point $\xi = (U, V)$ (Silverman 1986; Skuljan et al. 1999) adapted to a Gaussian kernel function:

$$\hat{f}(\xi) = \frac{1}{n} \sum_{i=1}^n K(|\xi - \xi_i|, h\lambda_i),$$

where $\xi_i = (U_i, V_i)$, λ_i is the local dimensionless bandwidth parameter at point ξ_i , h is a general smoothing parameter, n is the number of data points $\xi_i = (U_i, V_i)$. The parameter λ_i at each point of the two-dimensional UV plane is defined as

$$\lambda_i = \sqrt{\frac{g}{\hat{f}(\xi_i)}}, \quad (2)$$

where g is the geometric mean of $\hat{f}(\xi_i)$:

$$\ln g = \frac{1}{n} \sum_{i=1}^n \ln \hat{f}(\xi_i). \quad (3)$$

Obviously, to determine λ_i from Eqs. (2)–(3), we must know the distribution $\hat{f}(\xi)$ which, in turn, can be determined if all λ_i are known. Therefore, the problem of finding the sought-for distribution is solved iteratively. As the first approximation, we use the distribution

obtained by smoothing the initial UV map with a band of an arbitrary fixed width. The optimal value of the parameter h can be found from the condition for the rms deviation of the estimator $\hat{f}(\xi)$ from the true distribution $f(\xi)$ being at a minimum. In contrast to Skuljan et al. (1999), to determine λ_i at each iteration, we used the values of the function $\hat{f}(\xi)$ determined not at the specified points ξ_i but at all points of an equidistant grid on which the smoothed UV distribution is sought. As our comparison showed, both smoothing methods yield approximately the same results, but, at the same time, our approach requires much less computation. The value of h for all maps was taken to be 5.0. To obtain each map, we made 20 iterations.

The sampling interval of the two-dimensional maps was chosen from a typical uncertainty in the U and V velocities (Skuljan et al. 1999). In our case, it is 2 km s^{-1} , since the velocity errors for most of the stars in the solar neighborhood (about 80%) do not exceed $\pm 1 \text{ km s}^{-1}$. The sampling interval of the maps in our analysis of the velocity distributions for age separated samples was taken to be $d = 2 \text{ km s}^{-1}$. In analyzing the “all” sample of stars, we chose $d = 1 \text{ km s}^{-1}$ from a large number of stars as an optimal one from the standpoint of providing the necessary detail of the derived smoothed distribution. To obtain distributions similar to the probability density distribution, the smoothed two-dimensional velocity distributions must be scaled by the factor $n \times s$, where $s = d \times d \text{ km}^2 \text{ s}^2$. The map size was 256×256 pixels at the square bin size $s = 2 \times 2 = 4 \text{ km}^2 \text{ s}^2$ in the first case and 512×512 pixels at $s = 1 \times 1 = 1 \text{ km}^2 \text{ s}^2$ in the second case.

Wavelet Analysis

To identify statistically significant signals of the main inhomogeneities in the distributions of UV velocities, we also use the wavelet transform technique. This is known as a powerful tool for filtering spatially localized signals (Chui 1997; Vityazev 2001).

The wavelet transform of a two-dimensional distribution $f(U, V)$ consists in its decomposition into analyzing wavelets $\psi(U/a, V/a)$, where a is the scale parameter that allows a wavelet of a particular scale to be selected from the entire family of wavelets characterized by the same shape ψ . The wavelet transform $w(\xi, \eta)$ is defined as a correlation function, so that we have one real value of the following integral at any given point (ξ, η) in the UV plane:

$$w(\xi, \eta) = \int_{-\infty}^{\infty} \int_{-\infty}^{\infty} f(U, V) \psi\left(\frac{U - \xi}{a}, \frac{V - \eta}{a}\right) dU dV,$$

which is called the wavelet coefficient at (ξ, η) . Obviously, in our case of finite discrete maps, their number is finite and equal to the number of square bins on the map.

As the analyzing wavelet, we use a standard wavelet called a Mexican hat (MHAT). A two-dimensional MHAT wavelet is given by

$$\psi(r/a) = \left(2 - \frac{r^2}{a^2}\right) e^{-r^2/2a^2}, \quad (4)$$

where $r^2 = U^2 + V^2$. Wavelet (4) is obtained by doubly differentiating the Gaussian function. The parameter a that specifies the spatial scale (width) of the wavelet ψ is analogous to the parameter σ in Eq. (1). The main property of the wavelet ψ is that its integral over U and V is equal to zero, which allows any inhomogeneities to be detected in the investigated distribution. If the distribution being analyzed is inhomogeneous, then all coefficients of the wavelet transform will be zero.

For our wavelet analysis of various samples in the planes of UV, VW, UW velocities and in the $(V, \sqrt{U^2 + 2V^2})$ plane, we chose the scale parameter a to be 8.37 km s^{-1} . The value of this parameter allowed us to reliably identify the most significant structural features of the velocity distribution that are the subject of our investigation. Note that for our analysis of the velocities in the $(V, \sqrt{U^2 + 2V^2})$ plane, the map size was 1024×1024 pixels, with the square bin size being $s = 1 \times 1 = 1 \text{ km}^2 \text{ s}^2$.

RESULTS

Figure 2a presents the UV -velocity distribution for the selected 16737 single stars (the “all” sample) obtained by the adaptive kernel method applied to the initial velocity distribution shown in Fig. 1. The contour lines are drawn with a uniform step equal to 2% of the distribution peak.

The classical Pleiades, $(U, V) = (-14, -23) \text{ km s}^{-1}$, Hyades, $(U, V) = (-43, -20) \text{ km s}^{-1}$, Sirius, $(U, V) = (-8, 2) \text{ km s}^{-1}$, and Coma Berenices, $(U, V) = (-11, -8) \text{ km s}^{-1}$, streams as well as the Hercules, $(U, V) = (-31, -49) \text{ km s}^{-1}$, stream are clearly distinguished in Fig. 2a. In addition, there is a blurred clump elongated along the U axis in a wide region $(U, V) \approx (37, -22) \text{ km s}^{-1}$. In the opinion of Antoja et al. (2008), the Wolf 630 peak $(U, V) = (25, -33) \text{ km s}^{-1}$ (Eggen 1996) and the nameless peak $(U, V) = (50, -25) \text{ km s}^{-1}$ (Dehnen 1998) are associated with this new clump. Francis and Anderson (2008) designated this clump as the α Ceti stream; the UV coordinates of the star α Ceti, $(U, V) = (25, -23) \text{ km s}^{-1}$, are also far from the characteristic clump center, as for Wolf 630. As a compromise, we suggest calling this structure the Wolf 630- α Ceti stream or branch.

Figure 2b presents the sections of map 2a perpendicular to the (U, V) plane that pass through the main peaks and that make $+16^\circ$ with the U axis if measured clockwise (this axis is designated in the figure as U); the distribution density in units of 7×10^{-4} is along the vertical axis. The orientation of the sections coincides with the direction of the “branches” detected on the smoothed maps (see also Skuljan et al. 1999; Antoja et al. 2008).

As we see from Fig. 2, the Hyades peak dominates in amplitude, although the Pleiades peak is integrally more powerful, as can be seen from the wavelet distribution for the “all” sample shown in Fig. 4.

Figure 3 present the UV -velocity distributions for eight samples (t1–t8) of F and G dwarfs as a function of the stellar age, which allow the evolution of the main peaks and clumps to be traced. We used a total of 6079 single stars with distance and age errors $e_\pi/\pi < 0.2$ and $e_\pi/\pi < 0.3$, respectively. The mean ages τ of samples t1–t8 are 1.2, 1.7, 2.2, 2.7, 3.4, 4.9, 7.2, and 11.2 Gyr, respectively. The numbers of stars in samples t1–t8 are 509, 1105, 1184, 823, 803, 558, 586, and 511, respectively. The step of the contour lines in Fig. 3 is 6.7% of the peak value.

As we see from Fig. 3, the ratio of the amplitudes of the main peaks changes with age. For example, for the samples of comparatively young stars (t1,t2,t3), the Hyades peak is dominant; the Pleiades peak is gradually enhanced with stellar age (t4,t5) and is already dominant for sample t6. The Hyades and Pleiades peaks form an elongated structure in the shape of a “branch” whose orientation remains unchanged. Such structures in the UV -velocity distribution for a large number of Hipparcos stars were first described by Skuljan et al. (1999).

Numerical simulations of the disk heating by stochastic spiral waves performed by De

Simone et al. (2004) showed that the stratification of the UV distribution into “branches” and peaks could be explained by irregularities in the Galactic potential rather than by irregularities in the star formation rate. As was shown by Fux (2001), the presence of a bar at the Galactic center gives rise to branches. It is currently believed that the formation of the Hercules branch is related precisely to the influence of a bar.

Figure 4 presents the wavelet maps of UV , UW , and VW velocities for the “all” sample. The contour lines are given on a logarithmic scale: 1, 2, 4, 8, 16, 32, 64, 90, and 99% of the peak value. Note that only the positive contours that describe the clump regions are shown on the maps. Since the negative values of the wavelet distributions describe the regions of a sparse distribution of stars, they are of no interest to us and are not shown in the figures. Such clumps as HR 1614 (U, V) = (15, -60) km s⁻¹ and no. 13 (U, V) = (50, 0) km s⁻¹ are marked in Fig. 4 according to the list by Dehnen (1998). In addition, clumps no. 8 (U, V) = (-40, -50) km s⁻¹, no. 9 (U, V) = (-25, -50) km s⁻¹, and no. 12 (U, V) = (-70, -50) km s⁻¹ fall into the Hercules stream, while clump no. 14 (U, V) = (50, -25) km s⁻¹ falls into the Wolf630- α Ceti stream. As a result, out of the 14 clumps marked in Dehnen (1998), we cannot confirm the presence of isolated clump no. 11 (U, V) = (-70, -10) km s⁻¹ in the region of “high velocity” stars. According to Navarro et al. (2004), the Arcturus stream is located in the fairly narrow interval $-150 \text{ km s}^{-1} < V < -100 \text{ km s}^{-1}$ and in the considerably wider interval $-150 \text{ km s}^{-1} < U < 150 \text{ km s}^{-1}$; thus, the region marked in Fig. 4 fits into these limits.

Figure 4 indicates features W1 and W2 for the Wolf 630- α Ceti branch and features H1 and H2 for the Hercules branch. According to these data, we selected the stars belonging to these features and calculated their mean ages and metallicities, which are given in Table 1. For the selection of stars, we used our probabilistic approach described in detail in Bobylev and Bajkova (2007b). Note that our samples were comparable in the number of stars — 525 and 625 stars are contained in the Wolf 630- α Ceti and Hercules branches, respectively. To calculate the means and dispersions listed in Table 1, we used only the stars with available age and metallicity estimates, in fact, these are F and G dwarfs; the constraints $e_\pi/\pi < 0.1$ and $e_\pi/\pi < 0.3$ were used.

The last columns in Table 1 give parameters of the 1σ ellipses: the semimajor and semiminor axes a_i and b_i as well as the angle β_i between the vertical and semimajor axes (measured from the vertical axis clockwise). The selection of stars with these parameters was made within the boundaries of the 3σ ellipses.

Note that no significant concentrations of stars are observed in the $W - U$ and $W - V$ planes outside the central “ellipse”.

Next, we apply a technique proposed by Arifyanto and Fuchs (2006) that consists in identifying velocity field inhomogeneities in the plane of $V, \sqrt{U^2 + 2V^2}$ coordinates. It allows low-power streams to be reliably identified in the range of high space velocities.

Figure 5 shows the wavelet distributions for the “all” sample in the $(V, \sqrt{U^2 + 2V^2})$ plane. The contour lines are given on a logarithmic scale: 0.05, 0.1, 0.2, 0.4, 0.8, 1.6, 3.2, . . . , 50, and 99% of the peak value. In Figs. 5–8, we give the stellar velocities relative to the local standard of rest (LSR) whose coordinates are $(U, V, W) = (10.0, 5.2, 7.2)$ km s⁻¹ (Dehnen and Binney 1998); the cited coordinates of the clumps are also given relative to the LSR. Figure 5 marks the AF06 stream with coordinates $(-80, 130)$ km s⁻¹ (Arifyanto and Fuchs 2006), the Arcturus stream with coordinates $(-125, 185)$ km s⁻¹ (Arifyanto and Fuchs 2006), and the KFR08 stream with coordinates $(-160, 225)$ km s⁻¹ (Klement et al. 2008). On this diagram, the Wolf 630- α Ceti stream merges with the Hyades-Pleiades branch.

Figure 6 presents the wavelet maps in $V, \sqrt{U^2 + 2V^2}$ coordinates for samples of F and G dwarfs as a function of the stellar age; the set of levels is similar to that in Fig. 5. As we see from the figure, a prominent clump of KFR08 stream stars is observed for sample t8, which includes the oldest stars considered. The central point in the KFR08 region marked on the plot (t8) has the eighth level; all of the remaining clumps at $\sqrt{U^2 + 2V^2} > 250 \text{ km s}^{-1}$ have one level fewer and, hence, their significance is considerably lower.

Still, it is interesting to note that there is a clump close to the KFR08 region in Fig. 6 for sample t4. However, the significance of the levels in this case is negligible, corresponding to the presence of only one or two stars. A special search showed that one star from sample t4, HIP 77946, for which $[\text{Fe}/\text{H}] = -0.83$ and $\tau = 2.5 \text{ Gyr}$ (Holmberg et al. 2007), falls into the neighborhood of KFR08 with a radius of 30 km s^{-1} .

Table 2 gives parameters of the stars that are probable members of the KFR08 stream. We selected the candidates for membership in this stream based on the distribution of the expanded “all” sample with $e_\pi/\pi < 0.15$ in the plane of $(V, \sqrt{U^2 + 2V^2})$ coordinates. As a result, 19 stars were selected from the neighborhood of the clump center with coordinates $(-159, 227) \text{ km s}^{-1}$ and a neighborhood radius of 30 km s^{-1} .

To determine the probability that each of the selected stars belonged to the KFR08 and Arcturus streams, we performed Monte Carlo simulations of the distribution of stars in the plane of $V, \sqrt{U^2 + 2V^2}$ coordinates by taking into account the random errors in the stellar space velocities. We generated 3000 random realizations for each star. In our simulations of the KFR08 and Arcturus streams, we took the following parameters of their distribution in the $V, \sqrt{U^2 + 2V^2}$ plane obtained by analyzing Fig. 5: (1) the coordinates of the centers are $(-159, 227) \text{ km s}^{-1}$ for KFR08 and $(-124, 178) \text{ km s}^{-1}$ for Arcturus; (2) the velocity dispersion is 5 km s^{-1} for both streams. The results of our simulations are reflected in Fig. 7 and in the last column of Table 2, which gives the probability that a star belongs to the KFR08 stream, p . Obviously, the probability that a star belongs to the Arcturus stream is $1 - p$. As we see from Table 2, eleven stars constituting the core of the KFR08 stream have probabilities $p \geq 0.99$ and only two stars have $p = 0.65$. The positions of these two stars (HIP 74033 and HIP 58357) are marked in Fig. 7. As we see from the figure, their random errors are such that they have almost equal chances of being attributed to both the KFR08 and Arcturus streams. Therefore, it is not surprising that the star HIP 74033 in Arifyanto and Fuchs (2006) was attributed to the Arcturus stream.

Since we have failed to find information about the metallicities of several stars from this sample in the literature, we calculated the metallicity indices based on Strömgren uvby? photometry from the compilation by Hauck and Mermilliod (1998) using the calibration by Schuster and Nissen (1989).

The distribution of U, V, W velocities for KFR08 stream members is shown in Fig. 8. As can be seen from this figure, the stars are located in a narrow range of velocities V and in wider ranges of U and W than are typical of the Arcturus stream stars (Navarro et al. 2004).

Figure 9 presents a color-absolute magnitude diagram for KFR08 stream members with the Yonsei-Yale (Yi et al. 2003) 11-, 13-, and 15-Gyr isochrones for $Z = 0.007$ ($[\text{Fe}/\text{H}] = -0.43$). We can see that the stream stars fall nicely on the 13-Gyr isochrone; the deviations are most pronounced only for two stars, HIP 87101 and HIP 93269. Our isochrone age estimate for the stream is in good agreement with the available age estimates for individual stars (Table 2).

DISCUSSION

(1) Using currently available data, we have been able to confirm the presence of main known clumps, streams, and branches in the stellar velocity field in the solar neighborhood and to trace the evolution of the velocity field for F and G dwarfs as a function of the stellar age. Note that there is a very wide range of stellar ages in each of the classical Pleiades, Hyades, Sirius, Coma Berenices, and Hercules streams (Fig. 3). This is in good agreement with the results of a detailed analysis of the metallicity distribution and age estimates for stars performed recently by Antoja et al. (2008) and Francis and Anderson (2008).

(2) The Wolf 630- α Ceti and Hercules streams are interesting in that they both could be produced by a common mechanism related to the influence of a bar at the Galactic center (Dehnen 1999, 2000; Fux 2001; Chakrabarty 2007). As can be seen from Fig. 3, both streams begin to manifest themselves at a mean age of the sample stars > 2 Gyr. They are most pronounced at a mean stellar age of ≈ 7 Gyr (sample t7). Using improved stellar age estimates from an updated version of the Geneva-Copenhagen survey (Holmberg et al. 2007, 2008) led to a noticeable shift of the mean stellar age for the Hercules branch in the direction of its decrease. For example, in Bobylev and Bajkova (2007a), where the age estimates from the first version of the catalog (Nordström et al. 2004) were used, a similar development of the Hercules branch was achieved at a mean age of the sample stars ≈ 8.9 Gyr.

According to the data by Taylor (2000), the mean stellar metallicity is $[\text{Fe}/\text{H}] = -0.11 \pm 0.02 \pm 0.15$ dex (the error of the mean and dispersion) for the Wolf 630 stream (≈ 40 stars selected according to Eggen's lists) and $[\text{Fe}/\text{H}] = -0.12 \pm 0.04 \pm 0.18$ dex (the error of the mean and dispersion) for the Hercules stream (≈ 10 stars).

An extensive analysis of the distribution of stars in age and metallicity in various streams performed recently by Antoja et al. (2008) showed that the highest (compared to other branches) stellar metallicity dispersion is characteristic of the Hercules branch. The mean and dispersion are $[\text{Fe}/\text{H}] = -0.15 \pm 0.27$ dex.

This structure was shown to be distinguished increasingly clearly in the form of a branch starting from an age of 2 Gyr. Our results are generally in good agreement with those of Antoja et al. (2008).

The mean stellar metallicity and age for features H1 and H2 of the Hercules stream as well as W1 and W2 of the Wolf 630- α Ceti branch (Table 1) are consistent with the hypothesis of a dynamical nature of the streams related to the influence of the Galactic bar. This is seen most clearly for features H1 and H2. Thus, for example, feature H1, which is closer to the local standard of rest, is youngest. Since young field stars fall into the samples under consideration, the mean ages of the streams are underestimated, especially for features W1 and W2.

Note that the existence of the HR 1614 clump cannot be explained only by the presence of a OSC remnant with an age of ~ 2 Gyr (De Silva et al. 2007), since this clump is traceable in the UV distributions for samples of considerably older stars. Thus, for example, it is clearly seen on the UV map for stars with an age of ≈ 7 Gyr (t7, Figs. 3 and 4), suggesting that the HR 1614 clump is an outgrowth of the Hercules branch and can be dynamical in nature.

(3) The KFR08 stream was discovered by Klement et al. (2008) from their analysis of the data on faint (compared to Hipparcos) stars of the RAVE experiment. These authors identified 15 stream candidates. Since the distances of the stars in the analyzed sample were estimated from photometric data, they are less reliable than the trigonometric distances of

Hipparcos stars. At the same time, Klement et al. (2008) analyzed 13440 stars from the first version of the Geneva-Copenhagen survey (Nordström et al. 2004) and showed that the presence of about 30 stars (among the Hipparcos stars) in the KFR08 clump might be expected in the $V, \sqrt{U^2 + 2V^2}$ plane. However, no specific stars were selected.

The number of candidates for membership in the KFR08 stream we found is in satisfactory agreement with the expected estimates. The results of our search based on more accurate data are of great interest in establishing the nature of the KFR08 stream. In contrast to the samples by Klement et al. (2008), our “all” sample contains not only dwarfs but also giants.

As a result, we can see the main-sequence turnoff on the color-absolute magnitude diagram for KFR08 stream members (Fig. 9), which increases the reliability of the stream age estimate (≈ 13 Gyr).

According to the available data (Table 2), the metallicity indices for an overwhelming majority of stars lie within a fairly narrow range, $-1 < [\text{Fe}/\text{H}] < -0.3$. A similar homogeneity is also observed for the stars of the Arcturus stream (Navarro et al. 2004). This is one of the arguments for a common nature of these two streams. Obviously, much greater statistics is required to make the final decision.

Note that Minchev et al. (2009) suggested an alternative hypothesis about the nature of the AF06, Arcturus, and KFR08 streams. It is based on the assumption that the disk has not yet relaxed and it is “shaken” after the disruption of the dwarf galaxy captured by our Galaxy; therefore, waves are observed in the plane of UV velocities.

CONCLUSIONS

Based on the most recent data, we studied the space velocity field of ≈ 17000 stars in the solar neighborhood. We used data from a new version of the Hipparcos catalogue (van Leeuwen 2007), stellar radial velocities from the OSACA (Bobylev et al. 2006) and PCRV (Gontcharov 2006) catalogs reduced to a common system, and improved estimates of the ages and metallicity indices for F and G dwarfs from an updated Geneva-Copenhagen survey (Holmberg et al. 2007, 2008).

We identified all of the main clumps, streams, and branches known to date using various approaches. Among the stars with a relatively low velocity dispersion, these are the Pleiades, Hyades, and Coma Berenices streams or branches. Among the stars with an intermediate velocity dispersion, these are the Hercules and Wolf 630- α Ceti branches. Among the stars with a high velocity dispersion, these are the Arcturus and AF06 streams (Arifyanto and Fuchs 2006) and the KFR08 stream (Klement et al. 2008).

Our attention was focused on the most poorly studied structures, the Wolf 630- α Ceti and Hercules branches, and on the KFR08 stream discovered quite recently.

The present view of the nature of the Wolf 630- α Ceti and Hercules streams is that they could be produced by the same mechanism related to the influence of a bar at the Galactic center. Indeed, these structures begin to manifest themselves as independent branches at a mean age of the sample stars > 2 Gyr, which is in conflict with the hypothesis of their origin based on the theory of stellar streams (Eggen hypothesis). Our estimates showed that the mean stellar ages of these structures are quite comparable and are 4–6 Gyr. We revealed now significant differences in the metallicities of the stars belonging to these streams.

We found 19 Hipparcos stars belonging to the new KFR08 stream and obtained an

isochrone age estimate for the stream, 13 Gyr. The homogeneity of the kinematics, chemical composition, and age of the sample stars is consistent with the hypothesis that the stream is a relic remnant of the galaxy captured and disrupted by the tidal effect of our own Galaxy. Data from the GAIA experiment will undoubtedly play a major role for a further study of this structure.

ACKNOWLEDGMENTS

We are grateful to the referees for helpful remarks that contributed to a improvement of the paper. The SIMBAD search database was very helpful in the work. This study was supported by the Russian Foundation for Basic Research (project no. 08–02–00400) and in part by the “Origin and Evolution of Stars and Galaxies” Program of the Presidium of the Russian Academy of Sciences and the Program for State Support of Leading Scientific Schools of Russia (NSh–6110.2008.2).

REFERENCES

1. T. Antoja, F. Figueras, D. Fernández, and J. Torra, *Astron. Astrophys.* 490, 135 (2008).
2. M. I. Arifyanto and B. Fuchs, *Astron. Astrophys.* 449, 533 (2006).
3. R. Asiain, F. Figueras, J. Torra, et al., *Astron. Astrophys.* 341, 427 (1999).
4. T. Bensby, S. Feltzing, I. Lundstöm, et al., *Astron. Astroph.* 433, 185 (2005).
5. T. Bensby, M.S. Oey, S. Feltzing, et al., *Astroph. J.* 655, L89 (2007).
6. V.V. Bobylev, *Pisma Astron. Zh.* 30, 185 (2004) [*Astron. Lett.* 30, 159 (2004)].
7. V.V. Bobylev and A.T. Bajkova, *Astron. Zh.* 84, 418 (2007a) [*Astron. Rep.* 51, 372 (2007)].
8. V.V. Bobylev and A.T. Bajkova, *Pisma Astron. Zh.* 33, 643 (2007b) [*Astron. Lett.* 30, 571 (2004)].
9. V.V. Bobylev, G.A. Gontcharov, and A.T. Bajkova, *Astron. Zh.* 83, 821 (2006) [*Astron. Rep.* 50, 733 (2006)].
10. T.V. Borkova and V.A. Marsakov, *Astron. Zh.* 82, 453 (2005) [*Astron. Rep.* 49, 405 (2005)].
11. V. Castellani, S. DeglInnocenti, and P.Moroni, *Mon. Not. R. Astron. Soc.* 320, 66 (2001).
12. D. Chakrabarty, *Astron. Astrophys.* 467, 145 (2007).
13. E. Chereul, M. Crézé, and O. Bienaymé, *Astron. Astrophys.* 340, 384 (1998).
14. C.K. Chui, *Wavelets: A Mathematical Tool for Signal Analysis* (SIAM, Philadelphia, PA, 1997).
15. Ya.O. Chumak and A.S. Rastorguev, *Pisma Astron. Zh.* 32, 117 (2006a) [*Astron. Lett.* 32, 157 (2006)].
16. Ya.O. Chumak and A.S. Rastorguev, *Pisma Astron. Zh.* 32, 497 (2006b) [*Astron. Lett.* 32, 446 (2006)].
17. Ya.O. Chumak, A.S. Rastorguev, and S.J. Aarseth, *Pisma Astron. Zh.* 31, 342 (2005) [*Astron. Lett.* 31, 308 (2005)].
18. W. Dehnen, *Astron. J.* 115, 2384 (1998).
19. W. Dehnen, *Astrophys. J.* 524, L35 (1999).
20. W. Dehnen, *Astron. J.* 119, 800 (2000).
21. W. Dehnen and J.J. Binney, *Mon. Not. R. Astron. Soc.* 298, 387 (1998).

22. O.J. Eggen, *Astron. J.* 112, 1595 (1996).
23. B. Famaey, A. Jorissen, X. Luri, et al., *Astron. Astrophys.* 430, 165 (2005).
24. C. Francis and E. Anderson, *astro-ph: 0812.4032* (2008).
25. R. Fux, *Astron. Astrophys.* 373, 511 (2001).
26. G.A. Gontcharov, *Pisma Astron. Zh.* 32, 844 (2006) [*Astron. Lett.* 32, 759 (2006)].
27. B. Hauck and M. Mermilliod, *Astron. Astrophys. Suppl. Ser.* 129, 431 (1998).
28. A. Helmi, J.F. Navarro, B. Nordström, et al., *Mon. Not. R. Astron. Soc.* 365, 1309 (2006).
29. The HIPPARCOS and Tycho Catalogues, ESA SP-1200 (1997).
30. E. Hog, C. Fabricius, V.V. Makarov, et al., *Astron. Astrophys.* 355, L27 (2000).
31. J. Holmberg, B. Nordström, and J. Andersen, *Astron. Astrophys.* 475, 519 (2007).
32. J. Holmberg, B. Nordström, and J. Andersen, *astro-ph: 0811.3982* (2008).
33. A. Ibukiyama, and N. Arimoto, *Astron. Astrophys.* 394, 927 (2002).
34. J.S. Jenkins, H.R.A. Jones, Y. Pavlenko, et al., *Astron. Astrophys.* 485, 571 (2008).
35. J.R. King, A.R. Villarreal, D.R. Soderblom, et al., *Astron. J.* 125, 1980 (2003).
36. R. Klement, B. Fuchs, and H.-W. Rix, *Astrophys. J.* 685, 261 (2008).
37. A.H.W. Küpper, A. Macleod, and D. C. Hogg, *Mon. Not. R. Astron. Soc.* 387, 1248 (2008).
38. F. van Leeuwen, *Astron. Astrophys.* 474, 653 (2007).
39. T.E. Lutz and D.H. Kelker, *Publ. Astron. Soc. Pacific* 85, 573 (1973).
40. I. Minchev, A.C. Quillen, M. Williams, et al., *astro-ph: 0812.4032* (2009).
41. J.F. Navarro, A. Helmi, and K. Freeman, *Astrophys. J.* 601, L43 (2004).
42. B. Nordström, M. Mayor, J. Andersen, et al., *Astron. Astrophys.* 419, 989 (2004).
43. R.P. Olling and W. Dehnen, *Astrophys. J.* 599, 275 (2003).
44. A.C. Quillen and I. Minchev, *Astron. J.* 130, 576 (2005).
45. W. Schuster and P. Nissen, *Astron. Astrophys.* 221, 65 (1989).
46. W. Schuster, A. Moitinho, A. Marquez, et al., *Astron. Astrophys.* 445, 939 (2006).
47. G.M. De Silva, K.C. Freeman, J. Bland-Hawthorn, et al., *Astron. J.* 133, 694 (2007).
48. B.W. Silverman, *Density Estimation for Statistics and Data Analysis* (Chapman Hall, London, 1986).
49. R.S. De Simone, X. Wu, and S. Tremain, *Mon. Not. R. Astron. Soc.* 350, 627 (2004).
50. J. Skuljan, J.B. Hearnshaw, and P.L. Cottrell, *Mon. Not. R. Astron. Soc.* 308, 731 (1999).
51. D.R. Soderblom, B.F. Jones, S. Balachandran, et al., *Astron. J.* 106, 1059 (1993).
52. C. Soubiran, O. Bienaymé, T.M. Mishenina, et al., *Astron. Astrophys.* 480, 91 (2008).
53. M. Steinmetz, T. Zwitter, A. Seibert, et al., *Astron. J.* 132, 1645 (2006).
54. B.J. Taylor, *Astron. Astrophys.* 362, 563 (2000).
55. J. Torra, D. Fernández, and F. Figueras, *Astron. Astrophys.* 359, 82 (2000).
56. V.V. Vityazev, *Wavelet Analysis of Time Series* (SPb. Gos. Univ., St.-Petersbourg, 2001) [in Russian].
57. S. K. Yi, Y.-C. Kim, and P. Demarque, *Astrophys. J. Suppl. Ser.* 144, 259 (2003).
58. M.V. Zabolotskikh, A.S. Rastorguev, and A.K. Dambis, *Pisma Astron. Zh.* 28, 516 (2002) [*Astron. Lett.* 28, 454 (2002)]

Table 1: Characteristics of the Wolf 630- α Ceti branch (features W1 and W2) and the Hercules stream (features H1 and H2)

Obj.	N_{\star}	[Fe/H], dex	Age, Gyr	U , km s $^{-1}$	V , km s $^{-1}$	W , km s $^{-1}$	a_i , km s $^{-1}$	b_i , km s $^{-1}$	β_i deg.
W1	88	-0.06 (0.20)	3.9 (2.7)	23	-28	-5	7.4	5.6	148 $^{\circ}$
W2	95	-0.13 (0.19)	3.6 (2.3)	41	-26	-8	8.9	6.3	120 $^{\circ}$
H1	136	-0.09 (0.17)	4.6 (3.2)	-33	-51	-8	14.2	5.4	103 $^{\circ}$
H2	71	-0.16 (0.27)	5.7 (3.4)	-77	-49	-7	21.2	7.9	80 $^{\circ}$

Note. N is the number of stars with available age and metallicity estimates, the velocities U, V , and W are given relative to the Sun (see Fig. 4), the corresponding dispersions are given for the mean metallicity indices and mean ages of the sample stars.

Table 2: Parameters of the Hipparcos stars that are probable members of the KFR08 stream

HIP		[Fe/H]	Ref	Age	$U \pm e_U$	$V \pm e_V$	$W \pm e_W$	p
5336		-0.84	(1)		-32 ± 1	-153 ± 1	-28 ± 1	1.00
15495		-0.36	(2)		58 ± 4	-174 ± 8	-3 ± 3	1.00
18235		-0.71	(3)	11	-16 ± 3	-161 ± 4	-19 ± 2	1.00
19143		-0.49	(2)		-140 ± 3	-143 ± 11	-42 ± 2	0.98
54469	*	-0.72	(4)	11	91 ± 5	-159 ± 16	-64 ± 16	1.00
55988					50 ± 4	-154 ± 6	-25 ± 4	0.99
58357	*	-0.71	(1)		-123 ± 16	-134 ± 23	45 ± 1	0.65
58708		-0.30			-14 ± 3	-160 ± 4	15 ± 1	0.99
58843		-0.80			122 ± 9	-138 ± 14	-58 ± 7	0.81
59785		-0.37			-117 ± 9	-136 ± 6	-109 ± 7	0.92
60747	*	-0.77	(6)		110 ± 7	-146 ± 14	91 ± 7	0.91
64920		-0.42			66 ± 5	-159 ± 5	43 ± 5	0.99
74033		-0.75	(4)	13	-113 ± 10	-132 ± 10	42 ± 7	0.65
81170	*	-1.26	(5)		-77 ± 2	-157 ± 9	-123 ± 3	0.99
87101		-1.31	(6)		-76 ± 5	-159 ± 18	-3 ± 2	0.91
93269					70 ± 3	-140 ± 1	-4 ± 3	0.99
93623		-0.60	(2)		130 ± 5	-149 ± 16	-20 ± 1	0.96
96185		-0.60	(4)	12	-56 ± 1	-156 ± 1	66 ± 1	1.00
117702		-0.43	(7)		12 ± 7	-159 ± 7	124 ± 5	0.99

Note. The age is in Gyr, the velocities U, V , and W are in km s^{-1} and are given relative to the LSR (Dehnen and Binney 1998); the asterisk * marks the candidates with $e_\pi/\pi < 0.15$; the stellar metallicities and age estimates were taken from the following papers: 1, Soubiran et al. (2008); 2, Ibukiyama, and Arimoto (2002); 3, Bensby et al. (2005); 4, Holmberg et al. (2007); 5, Borkova and Marsakov (2005); 6, Schuster et al. (2006); 7, Jenkins et al. (2008).

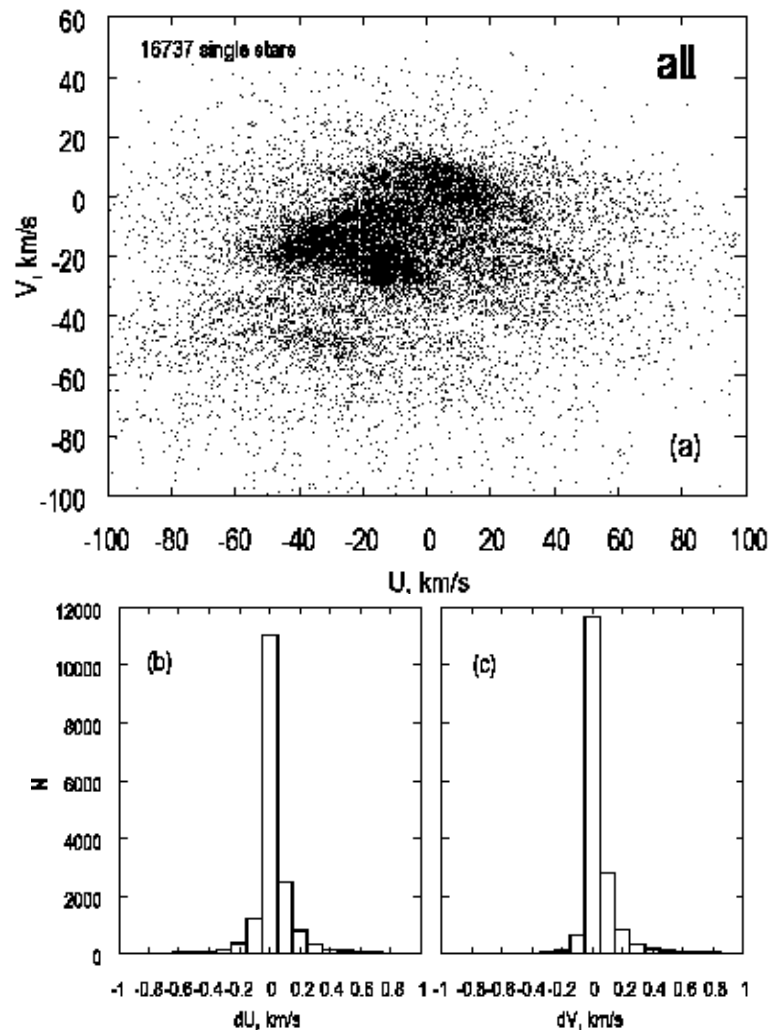


Fig. 1. (a) UV velocity distribution for the “all” sample of 16737 single stars with reliable distance estimates ($e_\pi/\pi < 0.1$); the velocities are given relative to the Sun. Distributions of the (b) U and (c) V velocity biases caused by the measurement errors of the stellar parallaxes.

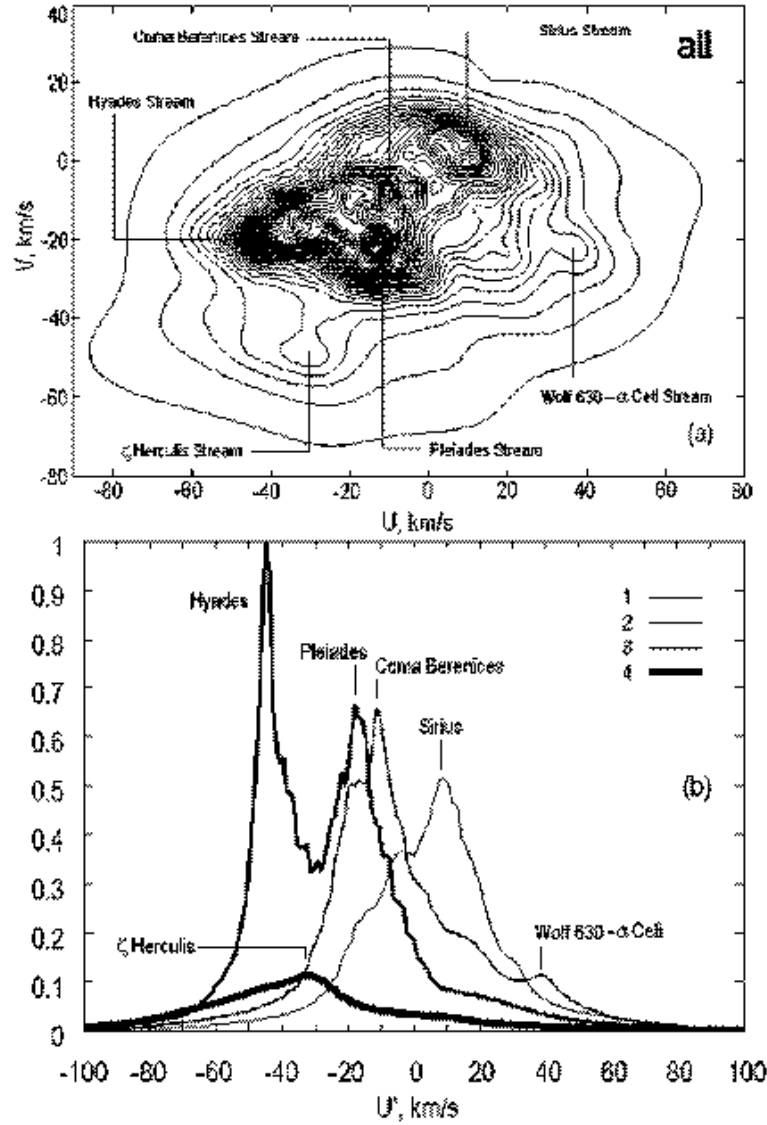


Fig. 2. Density of the UV -velocity distribution corresponding to Fig. 1 obtained by the adaptive kernel method; the velocities are given relative to the Sun (a); the sections of map (a) perpendicular to the (U, V) plane that pass through the main peaks and that make $+16^\circ$ with the U axis if measured clockwise (this axis is designated as U'); the distribution density in units of 7×10^{-4} is along the vertical axis, the numbers denote the sections passing through the Sirius (1), Coma Berenices (2), Pleiades-Hyades (3), and Hercules (4) branches (b).

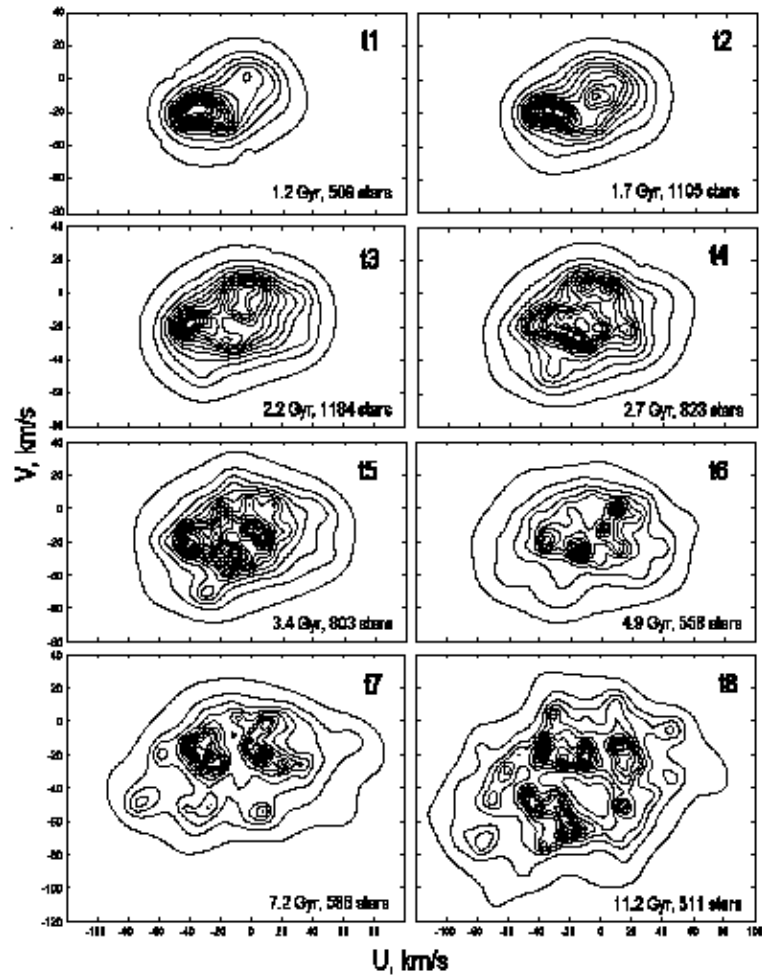


Fig. 3. Densities of the UV -velocity distribution for samples of F and G dwarfs as a function of the stellar age; the velocities are given relative to the Sun.

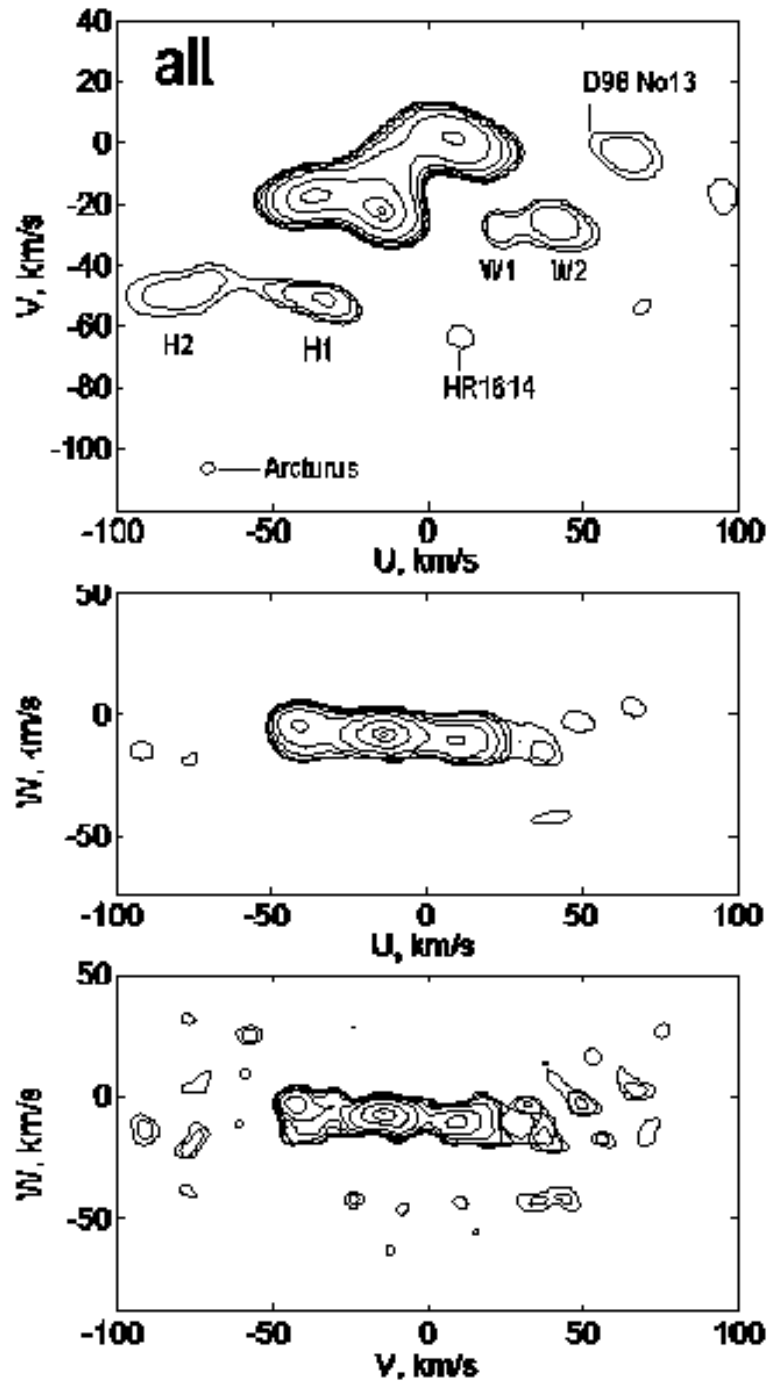


Fig. 4. Wavelet maps of UV , WU , and WV velocities for a sample of 16737 stars; the velocities are given relative to the Sun. See also the text.

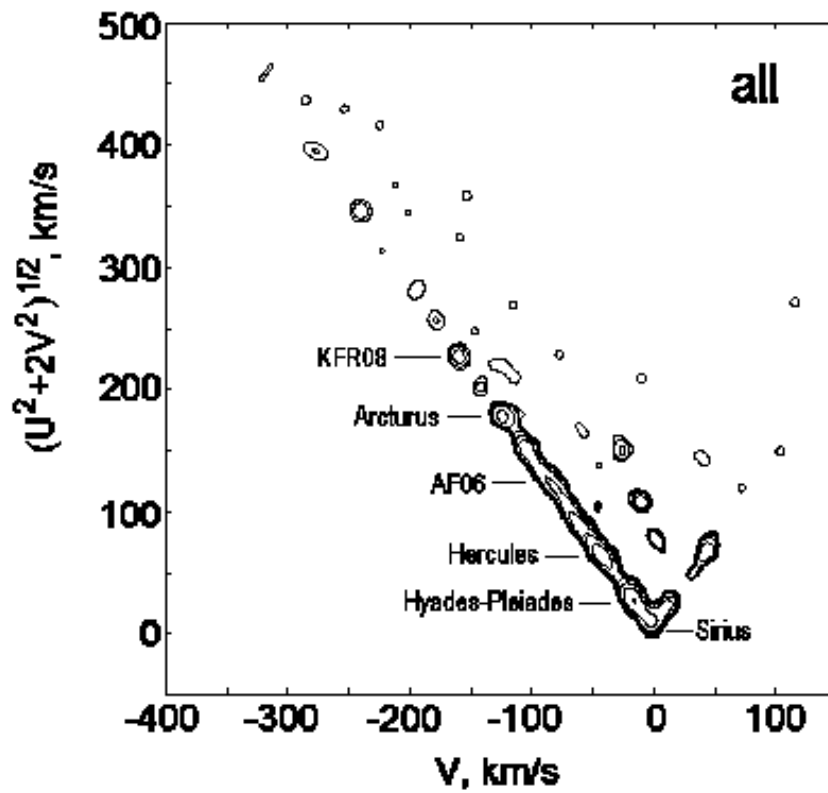


Fig. 5. Wavelet maps in the system of $(V, \sqrt{U^2 + 2V^2})$ coordinates for a sample of 16737 stars; the velocities are given relative to the LSR.

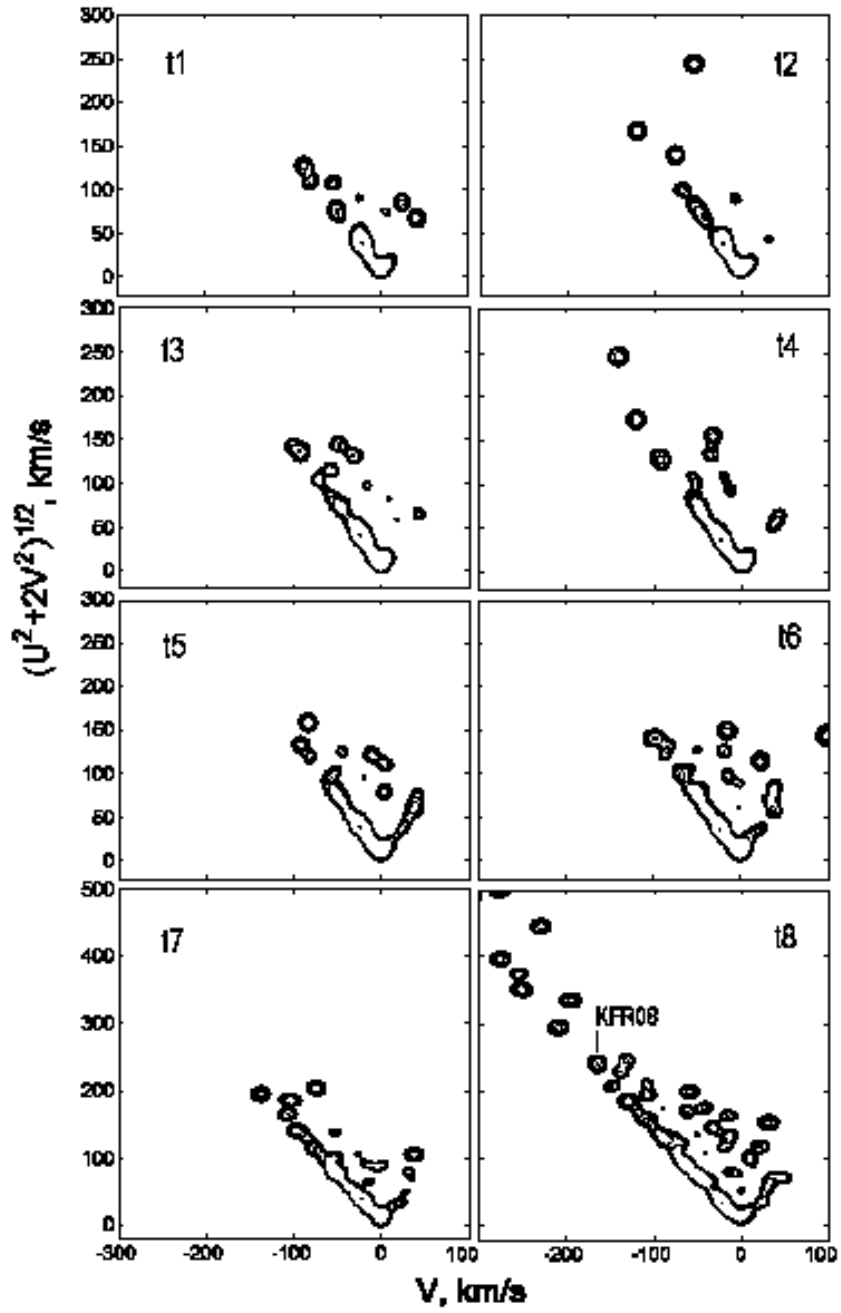


Fig. 6. Wavelet maps in the system of $(V, \sqrt{U^2 + 2V^2})$ coordinates for samples of F and G dwarfs as a function of the stellar age; the velocities are given relative to the LSR.

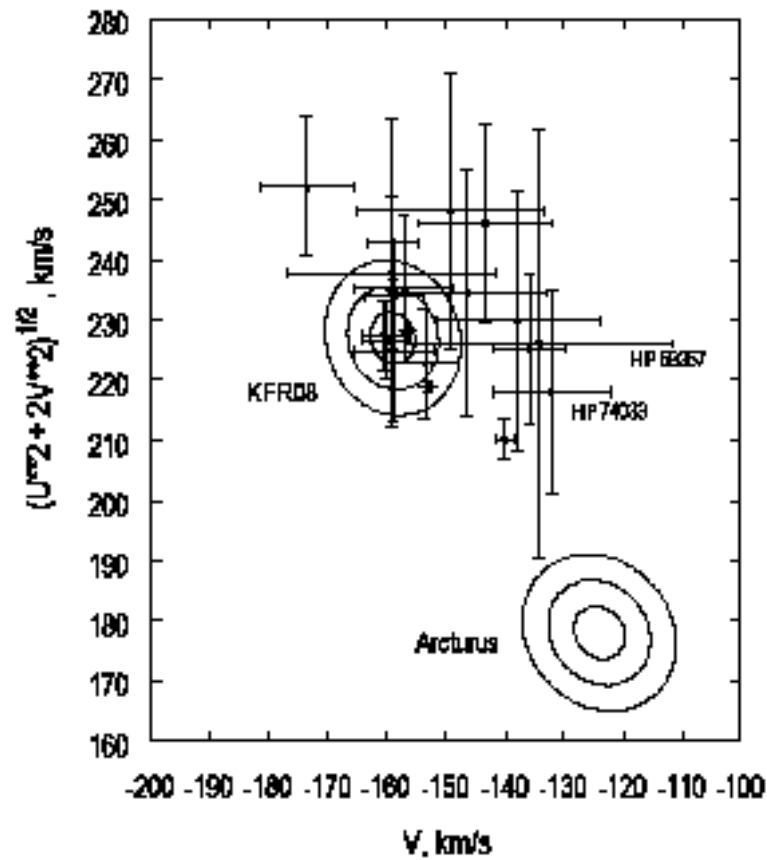


Fig. 7. Positions of KFR08 stream members in the $(V, \sqrt{U^2 + 2V^2})$ plane, the velocities are given relative to the LSR, three contours corresponding to probabilities of 0.683, 0.954, and 0.997 ($1\sigma, 2\sigma, 3\sigma$) are given for the KFR08 and Arcturus streams.

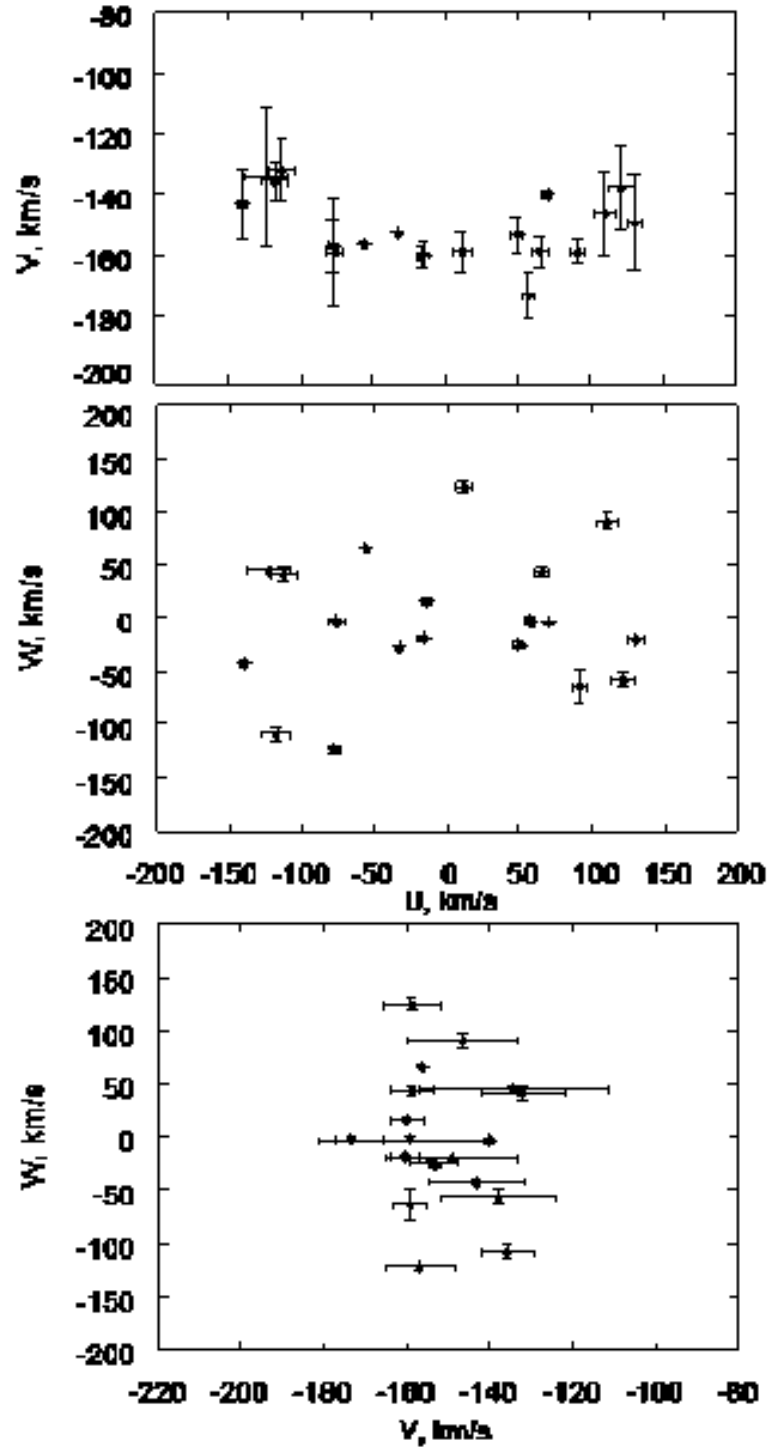


Fig. 8. Velocity distribution for KFR08 stream members, the velocities are given relative to the LSR.

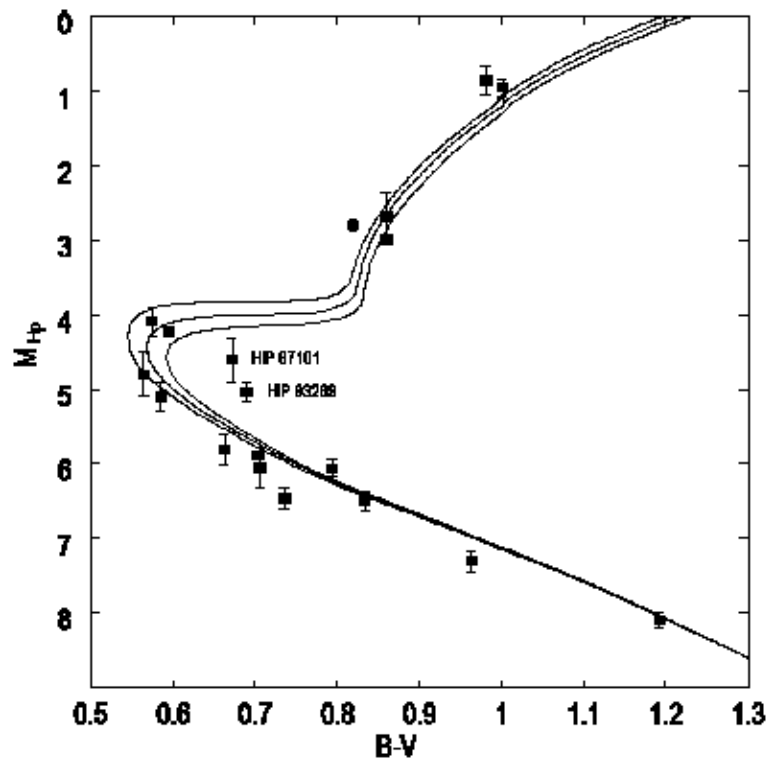


Fig. 9. Color-absolute magnitude diagram for KFR08 stream members.